Supporting Information

Yolk-Shell Structured $MnCo_2O_{4.5}$ Nanospheres for High Performance Lithium-Ion Battery Anodes

Yanhui Qiu, Jingchao Zhu, Xintao Zuo, Dapeng Liu, Yu Zhang

School of Chemistry, Beihang University, Beijing 100191, P. R. China

*Corresponding author. E-mail: liudp@buaa.edu.cn (D. P. Liu); jade@buaa.edu.cn (Y. Zhang)

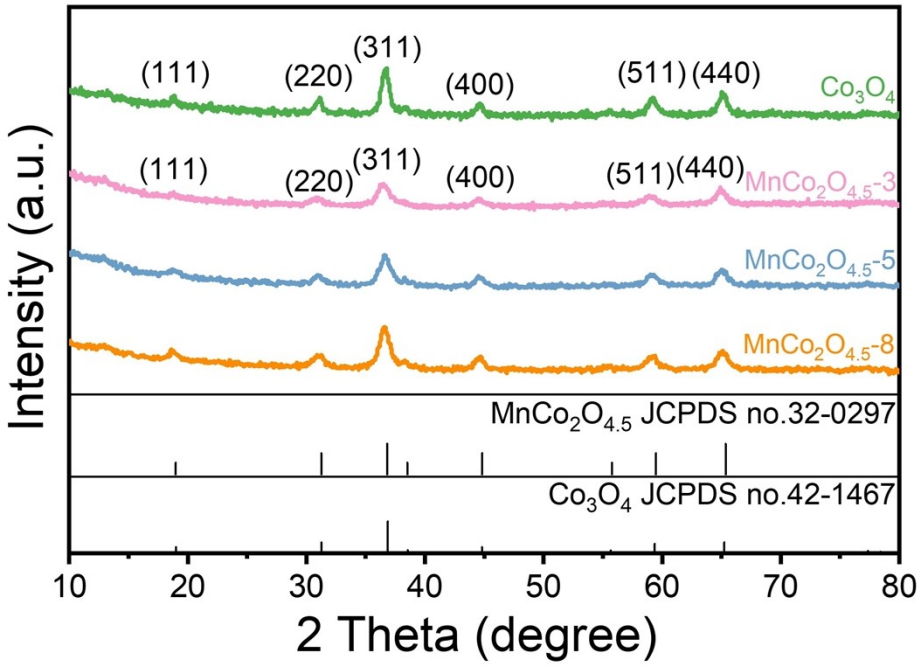

Fig. S1. XRD patterns of Co_3O_4, $MnCo_2O_{4.5}$-3, $MnCo_2O_{4.5}$-5, and $MnCo_2O_{4.5}$-8.

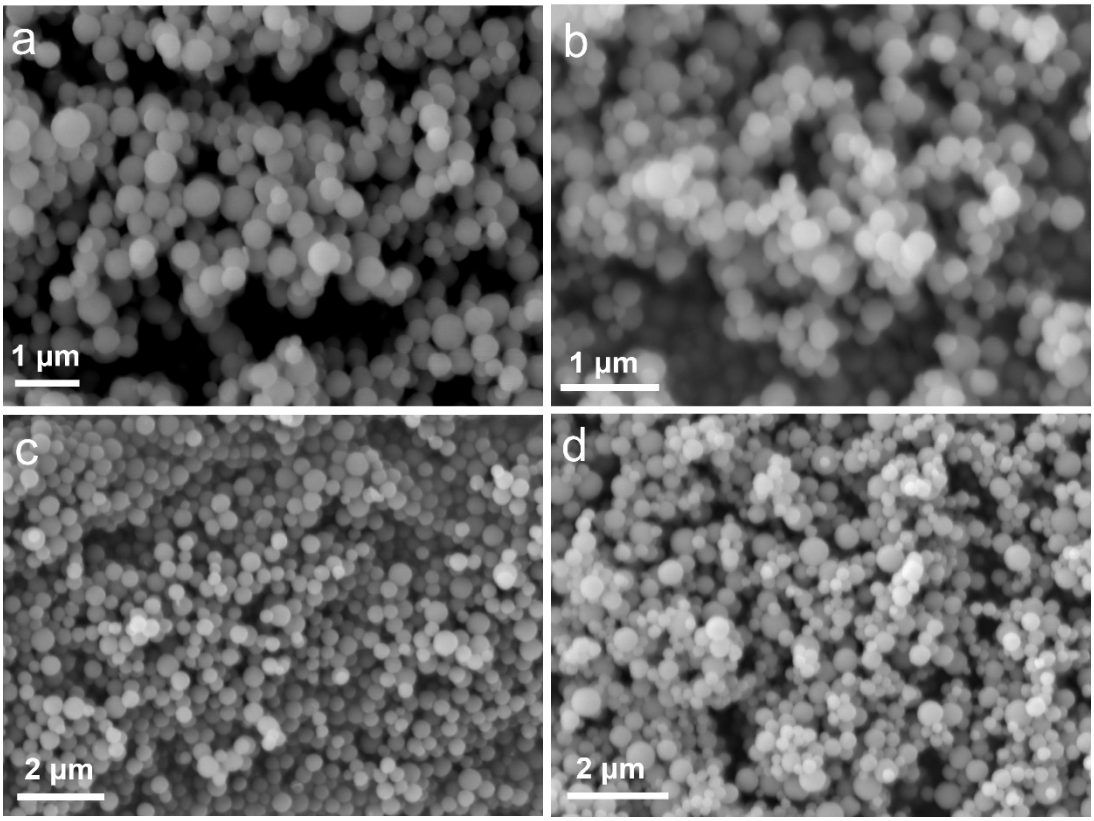

Fig. S2. SEM images of the precursors: (a) Co-gly, (b) CoMn-3-gly, (c) CoMn-5-gly, (d) CoMn-8-gly.

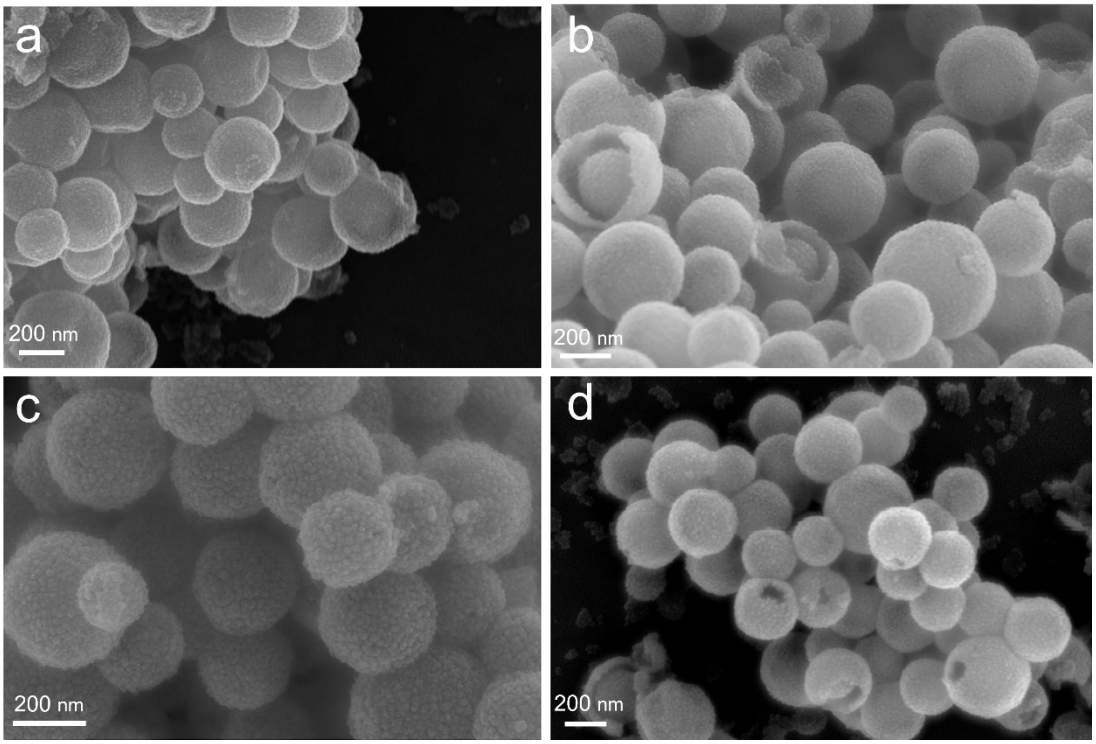

Fig. S3. SEM images of (a) Co_3O_4, (b) $MnCo_2O_{4.5}$-3, (c) $MnCo_2O_{4.5}$-5, (d) $MnCo_2O_{4.5}$-8.

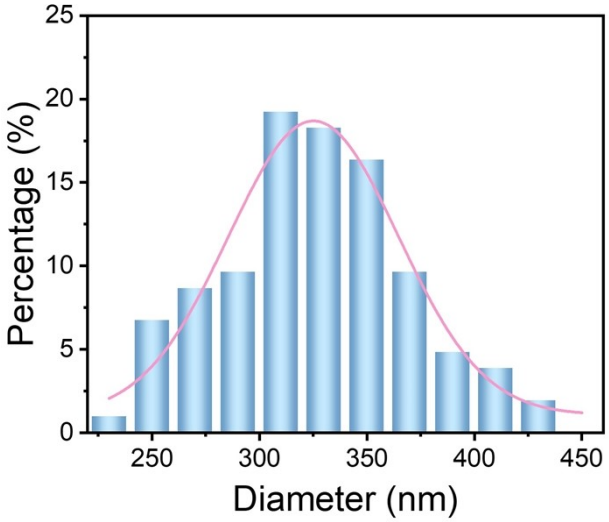

Fig. S4. $MnCo_2O_{4.5}$-5 particle size distribution diagram.

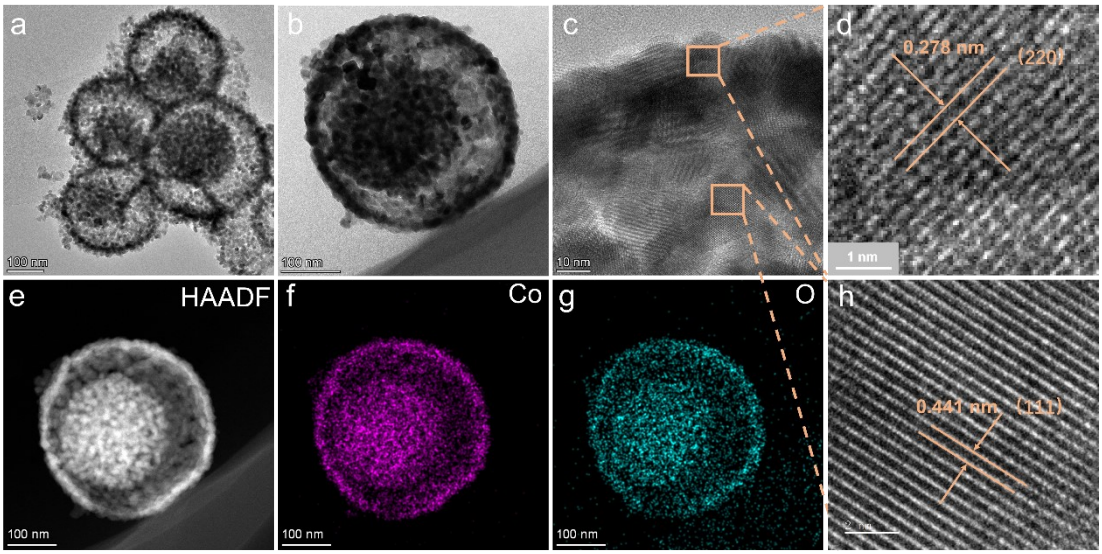

Fig. S5. (a, b) TEM images. (c) HRTEM image. (d) magnified view of the HRTEM image. (e) HAADF-STEM image, and (f, g, h) elemental distribution maps of Co_3O_4.

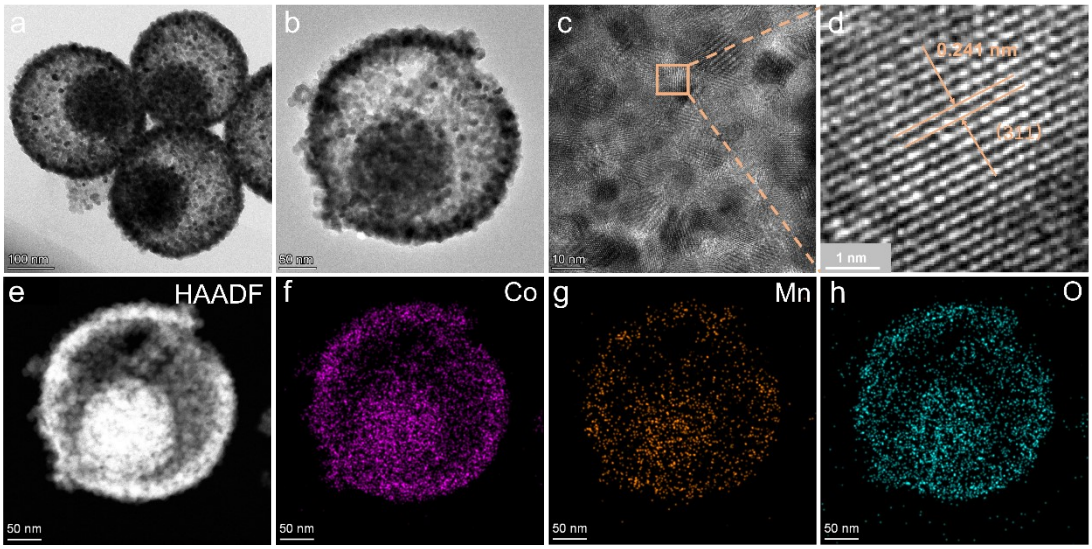

Fig. S6. (a, b) TEM images. (c) HRTEM image. (d) magnified view of the HRTEM image. (e) HAADF-STEM image, and (f, g, h) elemental distribution maps of $MnCo_2O_{4.5}$-3.

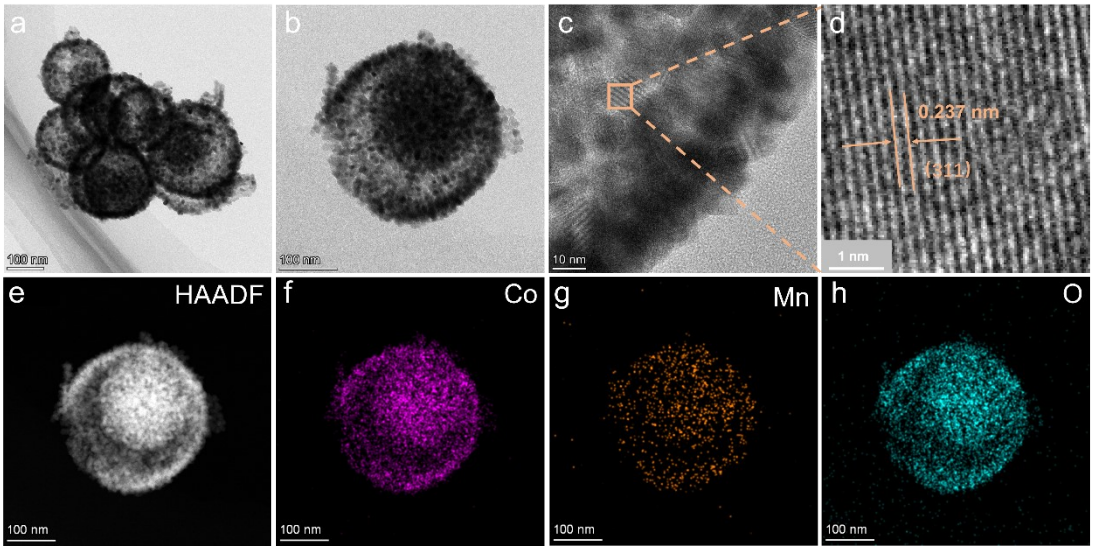

Fig. S7. (a, b) TEM images. (c) HRTEM image. (d) magnified view of the HRTEM image. (e) HAADF-STEM image, and (f, g, h) elemental distribution maps of $MnCo_2O_{4.5}$-8.

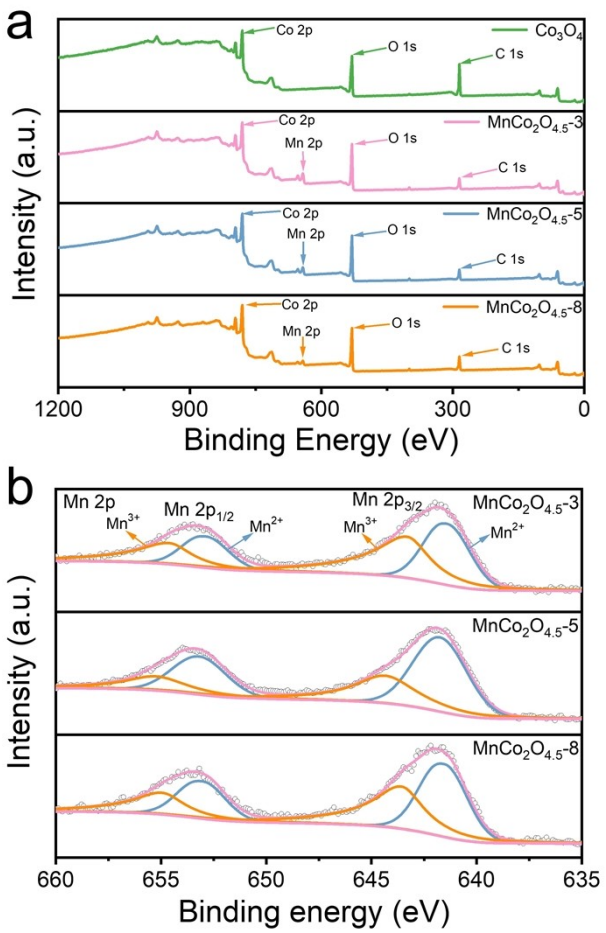

Fig. S8. (a) XPS survey spectrum. (b) XPS spectrum of Mn 2p.

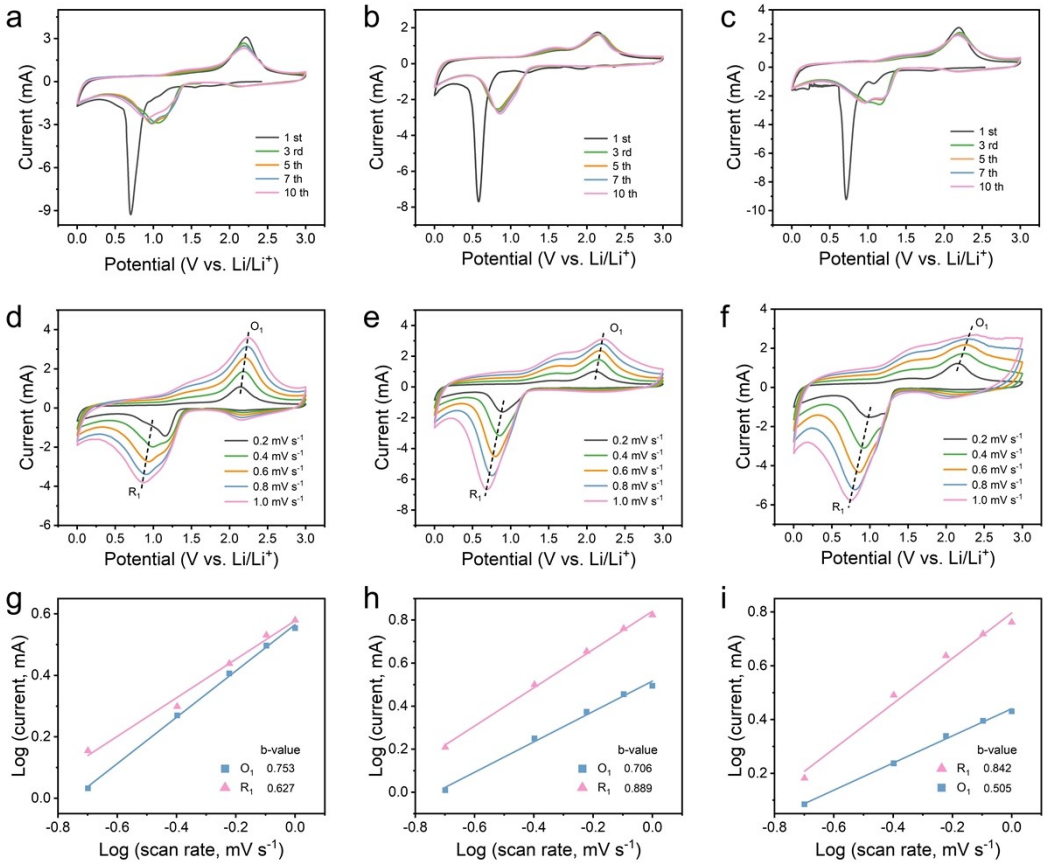

Fig. S9. CV curves of (a) Co_3O_4. (b) $MnCo_2O_{4.5}$-3. (b) $MnCo_2O_{4.5}$-8 at a scan rate of 0.5 mV s^{-1}. CV curves at various scanning rates of (d) Co_3O_4. (e) $MnCo_2O_{4.5}$-3. (f) $MnCo_2O_{4.5}$-8. (c) Log (i) vs. log (v) plots of (g) Co_3O_4. (h) $MnCo_2O_{4.5}$-3. (i) $MnCo_2O_{4.5}$-8.

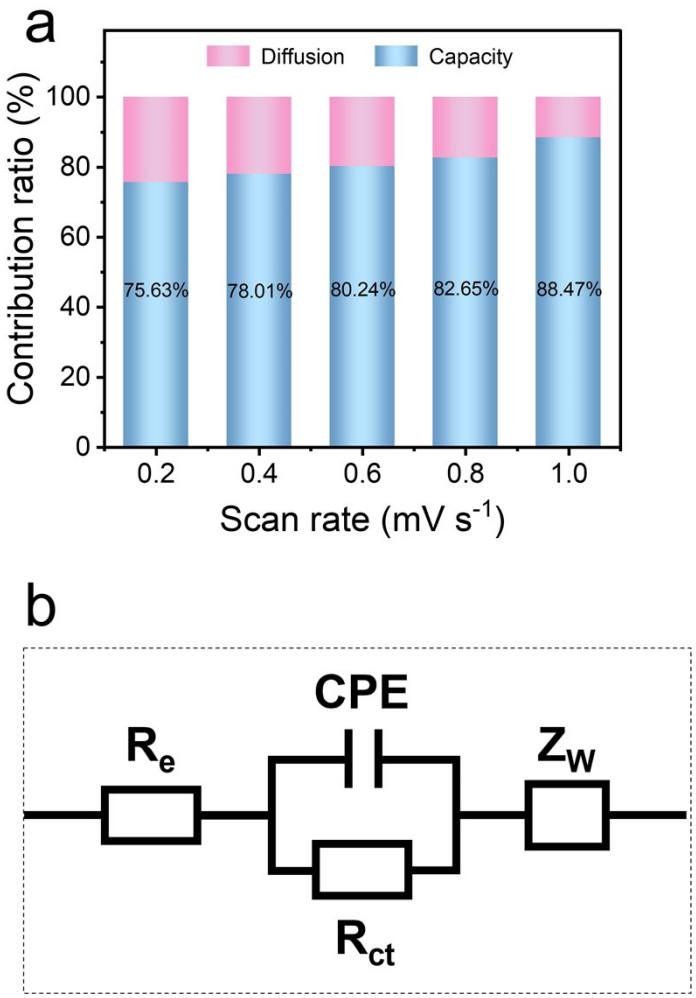

Fig. S10. (a) Percentage of pseudo-capacitive contribution of Co_3O_4 at all scan rates. (b) Equivalent circuit diagram. (Re: The internal resistance of electrolyte; Rct: The charge-transfer resistance.)

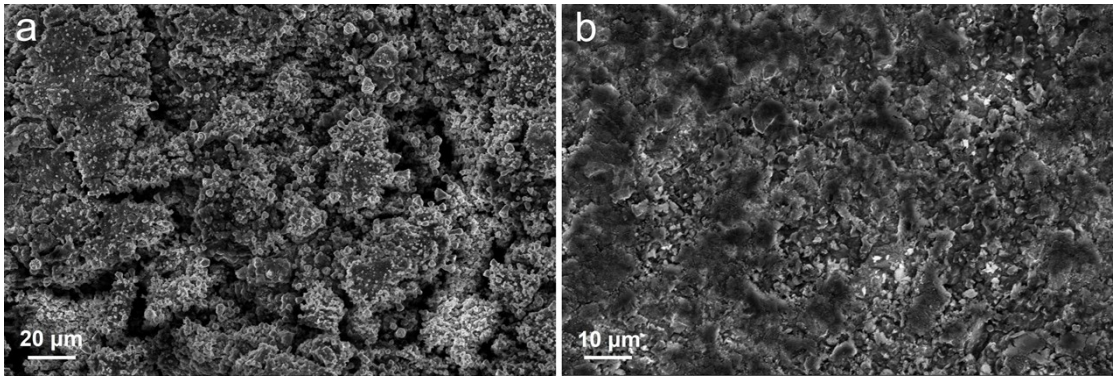

Fig. S11. SEM images of (a) $MnCo_2O_{4.5}$-5 and (b) Co_3O_4 after 400 cycles at 2 A g^{-1}.

Table S1. Comparison of electrochemical performance with various anodes for LIBs.

Materials	Current density ($A\ g^{-1}$)	Condition	Reversible capacity ($mAh\ g^{-1}$)	Ref.
CoO-ZnO@NC-450	0.2	After 100 cycles	796.2	[1]
Co_3O_4/CoP NFAs/CC	2.0	After 300 cycles	451.3	[2]
Co_3O_4/N–C	1.0	After 200 cycles	573	[3]
Co_3O_4/AG	0.5	After 100 cycles	510	[4]
NCF/Co_3O_4	1.0	After 300 cycles	576	[5]
Ge-Fe-O_x-700 NWs	0.1	After 50 cycles	750	[6]
NiFeP/C@rGO-21	1.0	After 300 cycles	530.4	[7]
$Co_{0.5}Fe_{2.5}O_4$/PCN	2.0	After 420 cycles	490	[8]
$NiCo_2S_4$@GS-1	5.0	Rate capability	460	[9]
Co_2AlO_4	3.2	Rate capability	548	[10]
$Ni_xCo_{3-x}O_4$	5.0	Rate capability	546	[11]
L-$ZnCo_2O_4$@rGO-30	3.2	Rate capability	686	[12]
$MnCo_2O_{4.5}$	0.2 2.0 5.0	After 50 cycles After 300 cycles Rate capability	1383.7 578.5 680.9	This work

References

1. Y. Liu, L. Wang, G. Chen, X. Miao, G. Wu, Z. Cao and Y. Zhang, Nitrogen-containing bimetal oxides derived from cobalt-zinc MOF as anode materials for lithium-ion batteries, *J. Phys. Chem. Solids*, 2024, **185**, 111728.
2. C. Zhao, L. Zhang, S. Jing, S. Kong, X. Zhang, X. Lan, Y. Feng, C. Liu, K. Tian, W. Gong and Q. Li, In Situ Construction of Heterostructured Co_3O_4/CoP Nanoflake Arrays on Carbon Cloth as Binder-Free Anode for High-Performance Lithium-Ion Batteries, *ACS Appl. Mater. Interfaces*, 2023, **15**, 23217-23225.
3. X. Han, W.-M. Chen, X. Han, Y.-Z. Tan and D. Sun, Nitrogen-rich MOF derived porous Co_3O_4/N-C composites with superior performance in lithium-ion batteries, *J. Mater. Chem. A*, 2016, **4**, 13040-13045.
4. H. Zeng, B. Xing, L. Chen, G. Yi, G. Huang, R. Yuan, C. Zhang, Y. Cao and Z. Chen, Nitrogen-Doped Porous Co_3O_4/Graphene Nanocomposite for Advanced Lithium-Ion Batteries, *Nanomaterials*, 2019, **9**, 1253.
5. R. Huang, Y. Li, Y. Song and L. Wang, Facial preparation of N-doped carbon foam supporting Co_3O_4 nanorod arrays as free-standing lithium-ion batteries' anode, *J. Alloy. Compd.*, 2020, **818**, 152839.
6. X. Zhong, H. Huan, X. Liu and Y. Yu, Facile synthesis of porous germanium-iron bimetal oxide nanowires as anode materials for lithium-ion batteries, Nano Res., 2018, **11**, 3702-3709.
7. Y. Wang, W. Xu, F. Liu, X. Li, J. Liu, K. Sun and R. Wang, Synergistic bimetallic phosphides and graphene enhancement NiFeP/C@rGO composites as high-performance anode for lithium-ion batteries, *Electrochim. Acta*, 2026, **545**, 147663.
8. D. Zhang, X. Li, J. Sun, Z. Huo, C. Zhang, Z. Cheng, F. Cao, B. Luo, G. Liu, X. Liu and C. Yu, A general and convenient strategy to construct spinel $A_xFe_{3-x}O_4$/porous carbon nanosheet (A = Co, Cu, Mn, Mg, Fe) composites as anodes for lithium ion batteries, *Electrochim. Acta*, 2025, **538**, 146927.
9. H. Chen, X. Ma and P. K. Shen, $NiCo_2S_4$ nanocores in-situ encapsulated in graphene sheets as anode materials for lithium-ion batteries, *Chem. Eng. J.*, 2019, **364**, 167-176.
10. K. Zeng, L. Tan, X. Li, Z. Wang, H. Guo, J. Wang and G. Yan, Mono-Active Bimetallic Oxide Co_2AlO_4 with Yolk-Shell Structure as a Superior Lithium-Storage Material, *ChemElectroChem*, 2019, **6**, 3298-3302.
11. L.-L. Wu, Z. Wang, Y. Long, J. Li, Y. Liu, Q.-S. Wang, X. Wang, S.-Y. Song, X. Liu and H.-J. Zhang, Multishelled $Ni_xCo_{3-x}O_4$ Hollow Microspheres Derived from Bimetal-Organic Frameworks as Anode Materials for High-Performance Lithium-Ion Batteries, *Small*, 2017, **13**, 1604270.
12. L. Li, Z. Xie, G. Jiang, Y. Wang, B. Cao and C. Yuan, Efficient Laser-Induced Construction of Oxygen-Vacancy Abundant Nano-$ZnCo_2O_4$/Porous Reduced Graphene Oxide Hybrids toward Exceptional Capacitive Lithium Storage, *Small*, 2020, **16**, 2001526.